Gyrotactic mechanism induced by fluid inertial torque for settling elongated microswimmers

Jingran Qiu[1], Zhiwen Cui[1], Eric Climent[2], and Lihao Zhao[1,*]

[1]*AML, Department of Engineering Mechanics, Tsinghua University, 100084 Beijing, China*

[2]*Institut de Mécanique des Fluides de Toulouse (IMFT), UMR5502 Université de Toulouse, CNRS, Allée du Prof. Camille Soula, 31400 Toulouse, France*

(Received 11 March 2021; revised 5 July 2021; accepted 8 April 2022; published 2 May 2022)

Marine plankton are usually modeled as settling elongated microswimmers. We consider the torque induced by fluid inertia on such swimmers, and we discover that they spontaneously swim in the direction opposite to gravity. We analyze the equilibrium orientation of swimmers in quiescent fluid and the mean orientation in turbulent flows using direct numerical simulations. Similar to well-known gyrotaxis mechanisms, the effect of fluid inertial torque can be quantified by an effective reorientation timescale. We show that the orientation of swimmers strongly depends on the reorientation timescale, and swimmers exhibit strong preferential alignment in an upward direction when the timescale is of the same order of the Kolmogorov timescale. Our findings suggest that the fluid inertial torque is a different mechanism of gyrotaxis that stabilizes the upward orientation of microswimmers such as plankton.

DOI: 10.1103/PhysRevResearch.4.023094

I. INTRODUCTION

Plankton play an important role in marine ecosystem. For instance, plankton produce oxygen by photosynthesis and transfer energy to zooplankton and other marine predators in the food web. Many motile plankton migrate vertically to pursue light or nutrients or to avoid predation [1–3]. The vertical migration is driven by gravity and other physical and chemical stimuli. The responses to these stimuli are known as gyrotaxis [4], phototaxis [5], chemotaxis [6], etc. Gyrotaxis is one of the important factors that influences the direction and efficiency of vertical migration [4]. Bottom-heaviness [7] and fore-aft asymmetry [8] are two well-known mechanisms of gyrotaxis. Many plankton are denser or wider at their rear parts than the front parts, and they are subjected to stabilizing torques due to gravity that reorients them in the upward direction. Based on these two mechanisms, gyrotactic swimmers are widely studied by modeling them as pointwise motile particles that swim relative to the fluid under a gravitational torque [9–16].

Gyrotaxis causes swimmers to preferentially swim in a vertical direction [7,14,17,18] and to form spatial clustering [10,12,15,16]. The magnitude of gyrotactic torque is crucial to these phenomena, influencing not only the orientation but also the intensity and location of patchiness. To quantify gyrotaxis, it is important to identify possible mechanisms of gyrotaxis and quantify their contributions. However, the question remains whether there exist other mechanisms for gyrotaxis. In particular, the widely used point-particle model neglects the effect of fluid inertial torque.

Recent studies indicated that the orientation of a spheroidal particle is affected by a fluid inertial torque [19,20]. This torque is a result of a convective fluid inertial effect when a particle moves relative to the local fluid [21]. Motile plankton are usually modeled as swimmers which move relative to the local fluid. The relative motion is due to their motility and the effect of gravitational settling, which results in a nonzero fluid inertial torque on settling microswimmers such as plankton. Interestingly, we find that elongated settling microswimmers reorient themselves in an upward direction under the influence of fluid inertial torque. Therefore, we suggest that fluid inertial torque is an alternative mechanism of gyrotaxis, which is different from the two well-known mechanisms of bottom-heaviness and fore-aft shape asymmetry.

In this paper, we introduce the model of settling swimmers and analyze their orientation in both quiescent and turbulent flows. We show that the magnitude of fluid inertial gyrotaxis depends on the shape and the swimming and settling speeds of swimmers, and can be quantified by a dimensionless parameter that measures the timescale of reorientation under fluid inertial torque.

II. FLUID INERTIAL TORQUE ON MICROSWIMMERS

Fluid inertial force and torque on a spheroid originate from the leading-order effects of fluid inertia when the spheroid moves relative to the fluid [21,22]. The Reynolds number of a planktonic swimmer, $\mathrm{Re}_\mathrm{p} = |\boldsymbol{u} - \boldsymbol{v}_\mathrm{p}|L/\gamma$, is usually much smaller than unity, where γ is the kinematic viscosity of fluid. The small Re_p is due to small size L and weak motility of the swimmer that yields a small velocity difference between the fluid $\boldsymbol{u}$ and the swimmer $\boldsymbol{v}_\mathrm{p}$. In the regime of $\mathrm{Re}_\mathrm{p} \ll 1$, the fluid inertial correction for force is negligible

*zhaolihao@mail.tsinghua.edu.cn

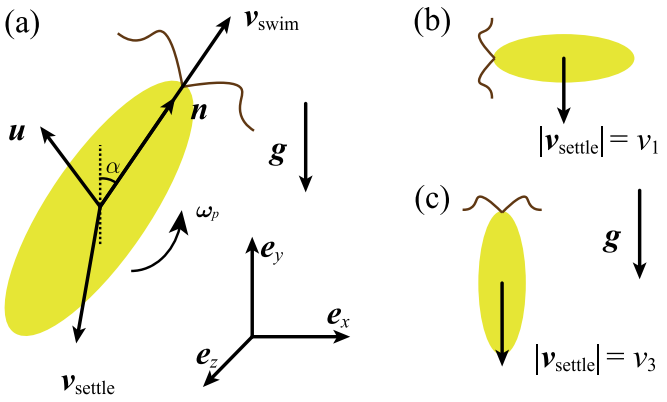

FIG. 1. (a) A sketch of a settling elongated swimmer. $\boldsymbol{e}_x$, $\boldsymbol{e}_y$, and $\boldsymbol{e}_z$ are the base vectors of the global frame of reference. (b) A swimmer settling with the symmetry axis perpendicular to gravity. (c) A swimmer settling with its symmetry axis parallel to the direction of gravity.

because its magnitude is of the order of $\mathrm{Re_p}$ and the swimmer experiences Stokes drag [19,22]. However, the fluid inertial torque can be significant compared to the Jeffery torque [23] that represents the effect of fluid velocity gradients on the rotation of swimmers. Reference [19] showed that the ratio between the magnitudes of inertial torque and Jeffery torque in turbulence is proportional to $|\boldsymbol{u} - \boldsymbol{v}_\mathrm{p}|^2/u_\eta^2$ [19], where u_η is the Kolmogorov velocity scale. Hence, the fluid inertial torque is not necessarily negligible when $\mathrm{Re_p} \ll 1$, especially when a swimmer moves relative to the fluid at a significant speed. A detailed dimensional analysis is provided in Appendix A.

Plankton usually satisfy the overdamped limit, which means that the response time of their motion is much shorter than the characteristic timescale of fluid motion [20]. In this case, plankton are usually modeled as pointwise spheroidal swimmers [9,10,12,14,15]. The inertia of a swimmer is neglected, so its translational and rotational motion is governed by kinematic equations. Following a similar approach in Ref. [20], we obtain the model of a settling microswimmer (Fig. 1) with the influence of fluid inertial torque (see Appendix A for details). The motion of a swimmer is governed by the following equations:

$$\dot{\boldsymbol{n}} = \boldsymbol{\omega}_\mathrm{p} \wedge \boldsymbol{n}, \tag{1}$$

$$\boldsymbol{v}_\mathrm{p} = \boldsymbol{u} + v_\mathrm{swim}\boldsymbol{n} + \boldsymbol{v}_\mathrm{settle}. \tag{2}$$

Here, $\boldsymbol{\omega}_\mathrm{p}$ is the angular velocity of the swimmer, and $\boldsymbol{n}$ is the unit vector along its symmetry axis. The swimmer is assumed to swim at a constant speed in the direction of $\boldsymbol{n}$, and it is advected by the local fluid with velocity $\boldsymbol{u}$. Settling due to gravity is taken into account by adding a settling speed $\boldsymbol{v}_\mathrm{settle}$. In the overdamped limit, a swimmer settling in a fluid flow satisfies the Stokesian flow assumption, and the settling speed is expressed as [24]

$$\boldsymbol{v}_\mathrm{settle} = -v_1\boldsymbol{e}_y - (v_3 - v_1)(\boldsymbol{e}_y \cdot \boldsymbol{n})\boldsymbol{n}, \tag{3}$$

where v_1 and v_3 are the Stokesian terminal velocities of a spheroid in a quiescent fluid with its symmetry axis orientated orthogonal to and parallel to the gravity direction, respectively. We specify the direction of y-axis $\boldsymbol{e}_y$ as the direction opposite to gravity, i.e., $\boldsymbol{e}_y = -\boldsymbol{g}/|\boldsymbol{g}|$.

The swimmer's angular velocity is expressed as [20]

$$\boldsymbol{\omega}_\mathrm{p} = \frac{1}{2}\boldsymbol{\omega} + \frac{\lambda^2 - 1}{\lambda^2 + 1}(\boldsymbol{n} \wedge \mathbb{S} \cdot \boldsymbol{n}) + \frac{M}{\gamma}[v_\mathrm{swim}v_1(\boldsymbol{e}_y \wedge \boldsymbol{n}) - v_1v_3(\boldsymbol{e}_y \cdot \boldsymbol{n})(\boldsymbol{e}_y \wedge \boldsymbol{n})], \tag{4}$$

where the first two terms on the right-hand side originate from the Jeffery torque [23], which represent the contributions of local fluid vorticity $\boldsymbol{\omega}$ and strain rate $\mathbb{S}$, respectively. The aspect ratio λ is defined as the ratio of the lengths between the major and minor axes of the spheroidal swimmer, with $\lambda = 1$ for spheres and $\lambda > 1$ for elongated spheroids. The third term on the right-hand side of Eq. (4) is the contribution of fluid inertial torque, where the shape factor M only depends on λ. M is zero for spheres and negative for elongated spheroids, ranging from $M = 0$ for $\lambda = 1$, to $M \approx -0.1$ when λ ranges from 2 to 8 (see Appendix A). Therefore, spherical swimmers are not subjected to fluid inertial torque. The contribution of fluid inertial torque consists of two parts. For convenience, we call the term $Mv_\mathrm{swim}v_1(\boldsymbol{e}_y \wedge \boldsymbol{n})/\gamma$ the *swimming-settling term*, which denotes the coupling effect of swimming and settling. Similarly, we call $-Mv_1v_3(\boldsymbol{e}_y \cdot \boldsymbol{n})(\boldsymbol{e}_y \wedge \boldsymbol{n})/\gamma$ the *settling term*, which is only ascribed to the settling effect.

III. SWIMMERS IN A QUIESCENT FLUID

To understand how fluid inertial torque affects the orientation of swimmers, we first analyze angular dynamics in a quiescent fluid. Using Eq. (4), the rotation of a swimmer is described as

$$\frac{d\alpha}{dt} = \frac{M}{\gamma}(v_\mathrm{swim}v_1 \sin\alpha - v_1v_3 \cos\alpha \sin\alpha). \tag{5}$$

Here, α is the angle of $\boldsymbol{n}$ relative to $\mathbf{e}_y$ [Fig. 1(a)], and thus $n_y \equiv \boldsymbol{n} \cdot \boldsymbol{e}_y = \cos\alpha$. From Eq. (5), a swimmer has three equilibrium orientations:

$$\alpha_0^{(1)} = 0,\ \alpha_0^{(2)} = \arccos\frac{v_\mathrm{swim}}{v_3},\ \text{and}\ \alpha_0^{(3)} = \pi, \tag{6}$$

which correspond to (1) swimming upward against gravity, (2) swimming with a fixed angle relative to the gravity direction, and (3) swimming downward along the gravity direction, respectively. Derived from Eq. (5), the first-order linear equation of a small perturbation around the equilibrium orientations, δ_α, reads

$$\frac{d\delta_\alpha}{dt} = \frac{Mv_1v_3}{\gamma}(R_v \cos\alpha_0 - \cos 2\alpha_0)\delta_\alpha, \tag{7}$$

where $R_v = v_\mathrm{swim}/v_3$. The solution of Eq. (7) is

$$\delta_\alpha = \exp\left[\frac{Mv_1v_3}{\gamma}(R_v \cos\alpha_0 - \cos 2\alpha_0)t\right]. \tag{8}$$

Inserting Eq. (6) into (8), and with $M < 0$, we find $\alpha_0^{(3)}$ is always unstable and there is one and only one stable orientation between $\alpha_0^{(1)}$ and $\alpha_0^{(2)}$, depending on the value of R_v. In general, the stable orientation is $n_{y,0} = \min(1, R_v)$.

The dependence of $n_{y,0}$ on R_v is due to the competition between the swimming-settling term and the settling term,

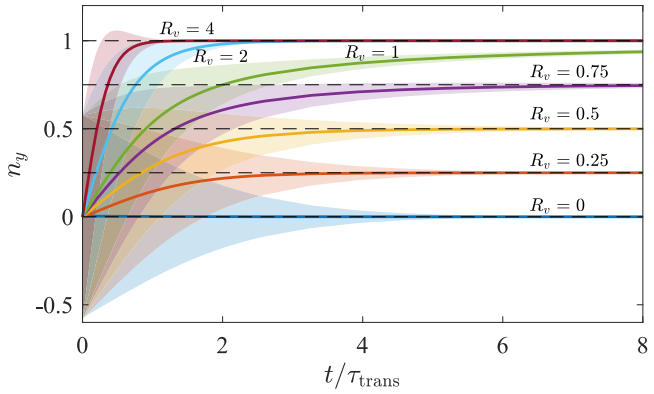

FIG. 2. Evolution of the orientation of swimmers n_y over dimensionless time $t/\tau_{\rm trans}$ in a quiescent fluid, where $\tau_{\rm trans} = \gamma/|M|v_1v_3$ is a timescale for the transient regime according to Eq. (8). Solid lines represent the mean value of n_y, and the colored areas represent the ranges of mean ± standard deviation. Horizontal dashed lines stand for the theoretical equilibrium orientation. Aspect ratio is $\lambda = 8$ for all cases here.

which make opposite contributions to the orientation. The swimming-settling term tends to align a swimmer in the upward direction, whereas the settling term tends to align the swimmer horizontally, as indicated in Refs. [19,20]. When $R_v < 1$, the swimming-settling term does not overcome the settling term, so the swimmer reaches an inclined orientation where the two terms are balanced. When $R_v \geqslant 1$, the swimming-settling term overcomes the settling term for any orientation, so the swimmer rotates to swim upward. Simulations in a quiescent fluid are performed to verify the aforementioned theoretical analysis. Figure 2 shows that swimmers with random initial orientation gradually approach the theoretical equilibrium orientation after a transient time. In the critical case of $R_v = 1$, swimmers takes a much longer time to approach the stable orientation because the swimming-settling term and the settling term are almost balanced at $n_y \approx 1$, resulting in a small angular velocity.

IV. EFFECTIVE REORIENTATION DUE TO FLUID INERTIAL TORQUE

Swimmers with $R_v \geqslant 1$ spontaneously swim in the upward direction, which are similar to the well-known gyrotactic swimmers with bottom-heaviness [7] or fore-aft asymmetry [8,25]. The similarity can also be deduced from Eq. (4). The fluid inertial term in Eq. (4) for elongated swimmers can be written as $-(\boldsymbol{e}_y \times \boldsymbol{n})/2B_I$, where

$$B_I = \frac{\gamma}{2|M|v_{\rm swim}v_1}\left[1 - \frac{v_3}{v_{\rm swim}}(\boldsymbol{e}_y \cdot \boldsymbol{n})\right]^{-1}. \tag{9}$$

This is similar to the widely used model of regular gyrotaxis, $-(\boldsymbol{e}_y \times \boldsymbol{n})/2B$ [12,15,26], where B is the reorientation timescale which quantifies how fast a swimmer recovers its stable orientation under gyrotactic torque. B_I can be regarded as an effective reorientation timescale provided by fluid inertial torque if $B_I > 0$.

Equation (9) shows some characteristics of B_I. First, only nonspherical, settling swimmers experience the effective gyrotaxis. Spherical or nonsettling swimmers have a zero M or v_1, which yields infinite B_I (zero fluid inertial torque). Second, B_I depends on the instantaneous orientation of a swimmer because of the contribution of the settling term. The dependence on orientation complicates the problem because the reorientation timescale varies along the trajectory as the swimmer rotates, and posterior knowledge of the mean orientation of the swimmers is required to estimate the magnitude of fluid inertial torque. However, B_I is almost constant if $\langle \boldsymbol{e}_y \cdot \boldsymbol{n}\rangle v_3/v_{\rm swim} \approx 0$, i.e., the settling term is negligible. This is justified when a swimmer swims much faster than it settles or when a swimmer has $\langle \boldsymbol{e}_y \cdot \boldsymbol{n}\rangle \approx 0$ along its trajectory. The first condition is true for typical plankton species (see Tables I and II in Appendix C), and the latter is true when fluid inertia torque is weak and the rotation of a swimmer is dominated by random turbulent fluctuations. When we neglect the settling term, B_I is expressed as

$$B_I \approx \frac{\gamma}{2|M|v_{\rm swim}v_1}. \tag{10}$$

With Eq. (10), we can quantify the magnitude of fluid inertial gyrotaxis. When a swimmer settles or swims faster, or when it has a larger M, it experiences a stronger gyrotactic effect caused by fluid inertial torque.

V. ORIENTATION OF SWIMMERS IN TURBULENCE

Planktonic microswimmers in the ocean or estuaries live in a turbulent environment, and their orientation controls the direction and efficiency of vertical migration. Therefore, it is necessary to understand how fluid inertial torque influences the orientation of swimmers in turbulence. We use Eulerian-Lagrangian direct numerical simulations to obtain the trajectories of swimmers in a forced homogeneous isotropic turbulence (HIT), and focus on the statistics of orientation. The HIT has a Taylor-Reynolds number $\mathrm{Re}_\lambda = u_{\rm rms}^2\sqrt{15/(\gamma\epsilon)} = 60$, where $u_{\rm rms}$ and ϵ are the root-mean-square velocity and dissipation rate, respectively. The incompressible Navier-Stokes equations are solved by a pseudospectral method with 96^3 grid points to ensure the accuracy of resolution at small scales. The statistics of each parameter configuration are obtained by averaging over 40 uncorrelated time samples of 120 000 trajectories. Details of the numerical methods are provided in Appendix B.

First, we need to quantify the magnitude of fluid inertial gyrotaxis relative to the turbulent motion. Turbulence influences the rotation of swimmers by the fluid velocity gradients along their trajectories, as shown in Eq. (4). The magnitude of the velocity gradients in a turbulent flow is of the order of Kolmogorov timescale τ_η. Thus, we normalize B_I with τ_η and obtain

$$\Psi_I \equiv B_I/\tau_\eta \approx (2|M|\Phi_{\rm swim}\Phi_{\rm settle})^{-1}, \tag{11}$$

where $\Phi_{\rm swim} = v_{\rm swim}/u_\eta$ and $\Phi_{\rm settle} = (2v_1 + v_3)/3u_\eta$ are the dimensionless swimming and settling speeds. Note that we assume $v_1 \approx v_3$ and thus $\Phi_{\rm settle} \approx v_1/u_\eta$ in Eq. (11) based on the fact that $1 \leqslant v_3/v_1 < 1.7$ for spheroids (see Appendix A). Similar to the parameter Ψ for gyrotaxis widely used in Refs. [12,14–16], Ψ_I quantifies the effective gyrotaxis provided by fluid inertial torque. According to the typical values

TABLE I. Parameters of typical plankton species [27,28,39–41]. Data are mean values ± standard deviations. Empty table cells represent unavailable data. Superscript[1]: V_{settle} is calculated using Stokes settling velocity assuming that the density of *Cochlodinium polykrikoides* is 5.9% greater than the fluid density [29].

Species		Width (μm)	Length (μm)	λ	v_{swim} (μm/s)	V_{settle}(μm/s)
Cochlodinium polykrikoides [39]	Single cell	25.1 ± 2.7	40.8 ± 2.0	1.63 ± 0.25	391 ± 92	26[1]
	2-cells	25.3 ± 1.8	50.7 ± 0.9	2.00 ± 0.18	599 ± 126	29[1]
	4-cells	25.5 ± 0.7	102.3 ± 4.2	4.01 ± 0.27	800 ± 129	42[1]
	8-cells	29.0 ± 1.4	182.0 ± 10.9	6.28 ± 0.68	856 ± 108	65[1]
Centropages typicus [28,41]	early nauplius	57.0 ± 11.5	132.0 ± 16.0	2.31 ± 0.19	330 ± 210	50 ± 40
	late nauplius	97.2 ± 22.1	225.0 ± 33.0	2.31 ± 0.19	720 ± 310	140 ± 70
Euterpina acutifrons [28]	late nauplius	86.6 ± 18.7	200.0 ± 27.0		1080 ± 310	260 ± 50
Eurytemora affinis [28]	late nauplius	87.4 ± 18.7	202.0 ± 27.0		1640 ± 400	182
Temora longicornis [28,40]	late nauplius	133.3 ± 26.3	308.0 ± 36.0		570 ± 140	240 ± 70
	copepod	129.0 ± 26.8	298.0 ± 38.0		820 ± 180	170 ± 240
Ceratium tripos [27]			73.5		167	164
Ceratium furca [27]			45.1		780	62
Akashiwo sanguinea [27]			42.2		300	54
Dinophysis acuminata [27]			32.4		332	32
Alexandrium minutum [27]			18.1		278	10
Prorocentrum minimum [27]			12.7		206	5

for oceanic plankton [9,11,27–29] (also see Appendix C), we investigate swimmers within a parameter space of $0 \leqslant \Phi_{\text{swim}} \leqslant 10$, $0 \leqslant \Phi_{\text{settle}} \leqslant 1$, and $1 \leqslant \lambda \leqslant 8$. In most of this parameter range, the settling term can be neglected because $\langle n_y \rangle v_3 / v_{\text{swim}} \approx 0$, as shown in Fig. 3(a). Accordingly, we calculate the range of Ψ_I using Eq. (11). Figure 3(b) shows that Ψ_I varies over two orders of magnitude in the present study. The decrease of Ψ_I at increasing Φ_{swim} and Φ_{settle} reflects that the ratio between the contributions of fluid inertial torque and Jeffery's torque increases as the relative velocity between the swimmer and the fluid grows.

Figure 4(a) shows the instantaneous spatial distribution and orientation of swimmers with $\Psi_I = 0.99$, $\lambda = 8$. We observe an obvious preferential alignment in the upward direction because the swimmers are subjected to a fluid inertial torque of the order of fluid velocity gradients. However, only elongated swimmers obtain upward orientation, as shown in Fig. 4(b). Equations (9)–(11) show that the reorientation time is proportional to $|M|^{-1}$. Spherical swimmers have $M = 0$, which indicates the fluid inertial torque vanishes and the reorientation time approaches infinity. In this case, the orientation of swimmers is almost isotropic, and $\langle n_y \rangle = 0$. On the contrary, elongated swimmers preferentially align in the upward direction. $|M|$ is nonmonotonous to λ, which reaches the maximum at about $\lambda = 4$ (see Appendix A). Therefore, among the four aspect ratios we considered, $\langle n_y \rangle$ is the largest when $\lambda = 4$ [Fig. 4(b)], in which case Ψ_I is minimal. We note that swimmers with $\lambda = 2$ already show a strong preferential orientation

TABLE II. Dimensionless numbers of typical plankton species shown in Table I. The Kolmogorov scales of ocean turbulence is calculated with $\gamma = 1.058 \times 10^{-6}$ m^2 s^{-1}, and the energy dissipation rate ϵ ranges from 1×10^{-9} to 1×10^{-6} m^2 s^{-3} [42]. Re_p is calculated with $\text{Re}_p = v_{\text{swim}} L / \gamma$ because $v_{\text{swim}} > V_{\text{settle}}$ for many species in Table I. Superscript[1]: The values are calculated with $\lambda = 2.3$ similar to *Centropages typicus*. Superscript[2]: The values are calculated with $\lambda = 2.0$.

Species		Φ_{swim}	Φ_{settle}	M	Re_p	St ($\times 10^{-5}$)	Ψ_I
Cochlodinium polykrikoides [39]	Single cell	2.17∼0.39	0.14∼0.03	−0.078	0.015	0.17∼5.52	20.7∼655.2
	2-cells	3.32∼0.59	0.1∼0.03	−0.101	0.029	0.22∼6.95	9.1∼287.2
	4-cells	4.44∼0.79	0.23∼0.04	−0.136	0.077	0.45∼14.11	3.6∼112.5
	8-cells	4.75∼0.84	0.36∼0.06	−0.137	0.147	0.90∼28.51	2.1∼67.4
Centropages typicus [28,41]	early nauplius	1.83∼0.33	0.28∼0.05	−0.114	0.041	1.29∼40.78	8.7∼274.2
	late nauplius	3.99∼0.71	0.78∼0.14	−0.114	0.153	3.75∼118.48	1.4∼44.9
Euterpina acutifrons [28]	late nauplius[1]	5.99∼1.06	1.44∼0.26	−0.114	0.204	2.96∼93.61	0.5∼16.1
Eurytemora affinis [28]	late nauplius[1]	9.09∼1.62	1.01∼0.18	−0.114	0.313	3.02∼95.49	0.5∼15.2
Temora longicornis [28,40]	late nauplius[1]	3.16∼0.56	1.33∼0.24	−0.114	0.166	7.02∼222.01	1.0∼33.1
	copepod[1]	4.55∼0.81	0.94∼0.17	−0.114	0.231	6.57∼207.83	1.0∼32.5
Ceratium tripos[2] [27]		0.93∼0.16	0.91∼0.16	−0.101	0.012	0.46∼14.60	5.9∼186.1
Ceratium furca[2] [27]		4.32∼0.77	0.34∼0.06	−0.101	0.033	0.17∼5.50	3.3∼105.9
Akashiwo sanguinea[2] [27]		1.66∼0.30	0.30∼0.05	−0.101	0.012	0.15∼4.81	9.9∼314.3
Dinophysis acuminata[2] [27]		1.84∼0.33	0.18∼0.03	−0.101	0.010	0.09∼2.84	15.2∼481.8
Alexandrium minutum[2] [27]		1.54∼0.27	0.05∼0.01	−0.101	0.005	0.03∼0.89	58.3∼1843.6
Prorocentrum minimum[2] [27]		1.14∼0.20	0.03∼0.00	−0.101	0.002	0.01∼0.44	159.8∼5053.4

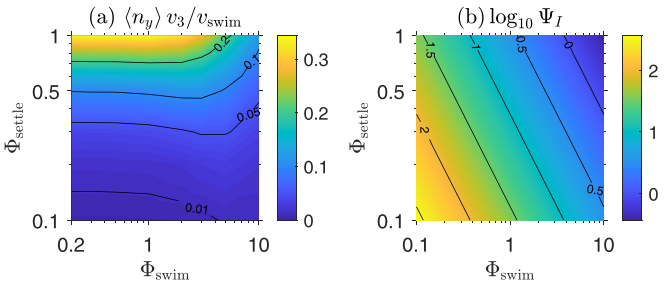

FIG. 3. (a) Value of $\langle n_y\rangle v_3/v_{\rm swim}$ in the parameter range of $\Phi_{\rm swim}$ and $\Phi_{\rm settle}$, using $\langle n_y\rangle$ of swimmers with $\lambda = 8$ as an example. (b) Value of Ψ_I calculated with Eq. (11) in the parameter range of $\Phi_{\rm swim}$ and $\Phi_{\rm settle}$ in the present study, with $M = -0.135$ corresponding to swimmers with $\lambda = 8$.

in the upward direction, which means fluid inertial torque can be significant even for slightly elongated swimmers.

Figure 4(c) shows the relation between Ψ_I and the orientation of swimmers. We observe that $\langle n_y\rangle$ is approximately proportional to Ψ_I^{-1}, suggesting a strong correlation between the orientation of swimmers and Ψ_I. The linearity is the best when Ψ_I is large, which can be explained by the probability distribution of orientation of the swimmers. For weak gyrotactic swimmers, the fluctuating turbulent velocity gradients act as Gaussian noises, and the rotation of gyrotactic swimmers is diffusive [17]. In this case, the orientation of spherical gyrotactic swimmers obeys an equilibrium

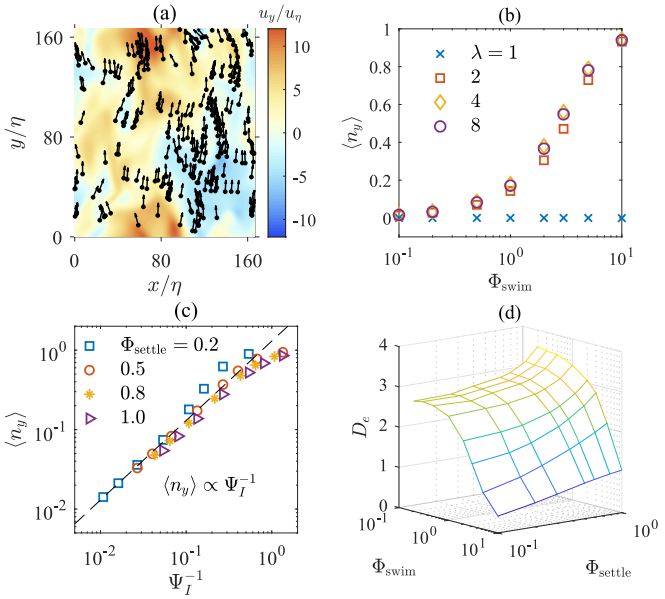

FIG. 4. (a) Instantaneous spatial distribution of swimmers in HIT. Black dots and tiny arrows stand for the position and swimming direction of each swimmer, respectively. Colors represent the vertical fluid velocity u_y. Quantities are normalized by Kolmogorov velocity and length scale, u_η and η, respectively. Parameters of swimmers are $\Phi_{\rm settle} = 0.5$, $\Phi_{\rm swim} = 10$, and $\lambda = 2$, corresponding to $\Psi_I = 0.99$. (b) $\langle n_y\rangle$ of swimmers with different aspect ratio and $\Phi_{\rm settle} = 0.5$ in HIT. (c) Mean orientation $\langle n_y\rangle$ vs Ψ_I^{-1} with $\lambda = 8$. The slope of the dashed line represents the relationship of $\langle n_y\rangle \propto \Psi_I^{-1}$. (d) D_e as a function of $\Phi_{\rm swim}$ and $\Phi_{\rm settle}$, obtained by the fitting distribution (12).

distribution [17,18],

$$g(n_y) = \frac{\beta e^{n_y/\beta}}{2\sinh\beta}, \text{ with } \beta = \frac{1}{\Psi\tau_\eta D_e}, \tag{12}$$

where Ψ is the gyrotactic parameter, and the effective rotation diffusivity D_e is determined by the time correlation of velocity gradients along the trajectories of swimmers, i.e., $D_e \sim \tau_{\rm cor}/\tau_\eta^2$ [17], where $\tau_{\rm cor}$ is the correlation time. Equation (12) is derived for spherical, nonsettling swimmers, but we have verified that Eq. (12) fits well with the distribution of settling elongated swimmers under fluid inertial torque in the present study. Figure 4(d) shows the best-fit D_e for different $\Phi_{\rm swim}$ and $\Phi_{\rm settle}$. D_e is expected to have little dependence on $\Phi_{\rm swim}$ and $\Phi_{\rm settle}$ when they are both much smaller than unity (which is the case for large Ψ_I). In this case, swimmers have small relative velocity with respect to the fluid and they almost follow streamlines. Therefore, the correlation timescale of fluid velocity gradients along their trajectories is $\tau_{\rm cor} \sim \tau_\eta$, so that $D_e \sim \tau_\eta^{-1}$ [17] and $\beta \sim \Psi^{-1}$. Moreover, the probability distribution (12) gives the mean orientation $\langle n_y\rangle = \coth\beta - \beta^{-1}$, which yields $\langle n_y\rangle \propto \beta$ for small β. This gives $\langle n_y\rangle \propto \Psi_I^{-1}$ for large Ψ_I, as shown in Fig. 4(c).

VI. CONCLUSIONS

The present study investigates the significance of fluid inertial torque on settling microswimmers owing to the velocity difference between the swimmers and fluid. The effect of fluid inertial torque shares a similar mathematical form with regular gyrotaxis mechanisms caused by bottom-heaviness or fore-aft asymmetry. The fluid inertial torque stabilizes the orientation of swimmers and allows them to swim in the upward direction spontaneously. Therefore, we suggest that fluid inertial torque is an effective mechanism of gyrotaxis for elongated settling swimmers.

The magnitude of fluid inertial torque depends on the shape, and swimming and settling speeds of a swimmer. Similar to Ref. [26], we quantify the gyrotactic effect produced by fluid inertial torque by B_I, which is an effective reorientation time measuring how fast a swimmer restores its stable orientation under fluid inertial torque. From B_I, we know some characteristics of fluid inertial gyrotaxis. First, only elongated, settling swimmers are subject to fluid inertial torque because they have nonzero shape factor M and settling velocity v_1 and v_3. Second, fluid inertial torque is stronger when swimmers swim and settle faster, in which case B_I is small. Third, B_I depends on the instantaneous orientation of swimmers due to the effect of settling term in Eq. (4), but in the limit of $v_{\rm swim} \gg v_3$, B_I is nearly independent with orientation and can be approximated by Eq. (10). This limit holds for typical plankton species and it allows for predicting B_I from the gaits of plankton without knowing their real-time orientation.

The orientation of swimmers under fluid inertial torque in turbulence is strongly related to the dimensionless parameter Ψ_I. When $\Psi_I \leqslant 1$, swimmers show strong alignment with upward direction, yielding $\langle n_y\rangle \approx 1$. When $\Psi_I \gg 1$, $\langle n_y\rangle \propto \Psi_I^{-1}$ as a result of the diffusive effect of turbulent fluid velocity gradients. We also show that swimmers with $\lambda = 2$ are strongly affected by fluid inertial torque, which implies that

fluid inertial torque can be significant even when swimmers are not strongly elongated.

Fluid inertial torque may have a potential impact on the gyrotaxis for elongated planktonic swimmers, especially for those forming long chains and thus having large swimming and settling speeds [27,30]. The settling effect of microswimmers was often neglected in previous studies [9–16]. However, our results demonstrate that neglecting settling will lead to an underestimation of gyrotaxis because fluid inertial torque vanishes without the settling effect. Moreover, unlike the two well-known gyrotaxis mechanisms which contribute to the rotation dynamics passively, the fluid inertial torque can be tuned by the swimming speed. This feature provides the possibility for microswimmers to actively control the gyrotactic reorientation time by adjusting their swimming velocity. As a different mechanism of gyrotaxis, swimmers under fluid inertial torque are also expected to sample specific flow regions and form local clustering as bottom-heavy gyrotactic swimmers do [12,14,16]. These phenomena are known to be controlled by the dimensionless reorientation time Ψ and the swimming speed Φ_{swim}. In the case with fluid inertial torque, one has to consider the influence of settling as well because it influences the reorientation time Ψ_I.

The present study focuses on the fluid inertial torque induced by the relative velocity between swimmer and local fluid. We note that the current swimmer model is still idealized. For instance, it neglects the influence of fluid velocity gradients and unsteadiness on the fluid inertial torque [31,32]. These effects could be important for swimmers in flows with strong shear and deserve to be studied in the future.

ACKNOWLEDGMENTS

This work was supported by the National Natural Science Foundation of China (Grants No. 11911530141 and No. 91752205). J.Q. and L.Z. acknowledge the support from the Institute for Guo Qiang of Tsinghua University (Grant No. 2019GQG1012).

APPENDIX A: INERTIALESS POINT-PARTICLE MODEL FOR A SETTLING SWIMMER

Following Refs. [19,20], here we derive the governing equations for an elongated settling microswimmer [Eqs. (1)–(4)]. Newton's second law for a spheroidal particle is

$$m_{\text{p}}\frac{d\boldsymbol{v}_{\text{p}}}{dt} = \boldsymbol{F}, \tag{A1}$$

$$m_{\text{p}}\frac{d}{dt}[\mathbb{I}_p(\boldsymbol{n})\boldsymbol{\omega}_p] = \boldsymbol{T}. \tag{A2}$$

Here, m_{p} is the particle mass, m_{f} is the mass of fluid occupied by the particle, and $\boldsymbol{v}_p$ and $\boldsymbol{\omega}_p$ are the particle velocity and angular velocity, respectively. $\mathbb{I}_p = I_{p,ij}$ is the rotational inertia tensor per unit-mass of the particle,

$$I_{p,ij} = I_{\perp}(\delta_{ij} - n_i n_j) + I_{\parallel} n_i n_j, \tag{A3}$$

where $\boldsymbol{n}$ is the particle swimming direction, $I_{\perp} = a^2(1+\lambda^2)/5$ and $I_{\parallel} = 2a^2/5$, with a being the half length of the minor axis of the particle, and λ is the aspect ratio defined as the ratio between the length of the major and minor axes of the particle. The force on a swimmer reads

$$\boldsymbol{F} = \boldsymbol{F}_{\text{St}} + \boldsymbol{F}_I + F_{\text{swim}}\boldsymbol{n} + (m_{\text{p}} - m_{\text{f}})\boldsymbol{g}, \tag{A4}$$

$$\boldsymbol{F}_{\text{St}} = 6\pi a\rho_{\text{f}}\gamma\mathbb{A}(\boldsymbol{u} - \boldsymbol{v}_p), \tag{A5}$$

$$\boldsymbol{F}_I = \frac{9\pi}{8}\rho_{\text{f}}a^2\max(\lambda, 1)|\boldsymbol{v}_{\text{p}} - \boldsymbol{u}| \times [3\mathbb{A} - \mathbb{I}(\hat{\boldsymbol{u}}_s \cdot \mathbb{A}\hat{\boldsymbol{u}}_s)]\mathbb{A}(\boldsymbol{u} - \boldsymbol{v}_{\text{p}}). \tag{A6}$$

The total force is the summation of Stokes drag force $\boldsymbol{F}_{\text{St}}$ [33], the fluid inertial correction of force, or so-called Oseen correction, $\boldsymbol{F}_I$ [22,34], the swimming propulsion force $F_{\text{swim}}\boldsymbol{n}$, and the contributions of gravity and buoyancy, $(m_{\text{p}} - m_{\text{f}})\boldsymbol{g}$. In Eq. (A5), ρ_{f} and γ are the density and kinematic viscosity of fluid, respectively, and $\boldsymbol{u}$ is the fluid velocity at the particle position. The translational resistant tensor $\mathbb{A}$ is defined as

$$A_{ij} = A_{\perp}(\delta_{ij} - n_i n_j) + A_{\parallel} n_i n_j, \tag{A7}$$

where $A_{\perp}$ and $A_{\parallel}$ depend only on the aspect ratio λ of a particle, and the expressions can be found in Refs. [20,35]. In Eq. (A6), $\hat{\boldsymbol{u}}_s = (\boldsymbol{u} - \boldsymbol{v}_{\text{p}})/|\boldsymbol{u} - \boldsymbol{v}_{\text{p}}|$.

The torque on a particle reads

$$\boldsymbol{T} = \boldsymbol{T}_J + \boldsymbol{T}_I, \tag{A8}$$

$$\boldsymbol{T}_J = 6\pi a\rho_{\text{f}}\gamma\mathbb{C}\left(\frac{1}{2}\boldsymbol{\omega} - \boldsymbol{\omega}_{\text{p}}\right) + 6\pi a\rho_{\text{f}}\gamma\mathbb{H} : \mathbb{S}, \tag{A9}$$

$$\boldsymbol{T}_I = F_\beta\rho_{\text{f}}a^3\max(\lambda, 1)^3 \times [\boldsymbol{n} \cdot (\boldsymbol{v}_{\text{p}} - \boldsymbol{u})][\boldsymbol{n} \wedge (\boldsymbol{v}_{\text{p}} - \boldsymbol{u})]. \tag{A10}$$

Here, the Jeffery torque $\boldsymbol{T}_J$ is related to the local fluid vorticity $\boldsymbol{\omega}$ and strain rate $\mathbb{S}$ [23], and $\mathbb{C}$ and $\mathbb{H}$ are rotational resistant tensors [20,35],

$$C_{ij} = C_{\perp}(\delta_{ij} - n_i n_j) + C_{\parallel} n_i n_j, \tag{A11}$$

$$H_{ijk} = H_0\epsilon_{ijl}n_k n_l, \tag{A12}$$

where $C_{\perp}$, $C_{\parallel}$, and H_0 are given in Refs. [20,35]. The fluid inertial torque $\boldsymbol{T}_I$ depends on both the magnitude and direction of the relative translational motion between particle and fluid [21], and thus influences the orientation of particles whenever they translate relative to the fluid, such as settling [19,20] or swimming. In Eq. (A10), F_β is a parameter depending only on λ [21].

Now, we can evaluate the relative importance of fluid inertial force and torque by comparing their magnitudes with those of other terms. For inertial force, $|\boldsymbol{F}_I|/|\boldsymbol{F}_{\text{St}}| \sim a|\boldsymbol{u} - \boldsymbol{v}_{\text{p}}|/\gamma = \text{Re}_{\text{p}}$. This suggests that $\boldsymbol{F}_I$ is negligible in the limit of $\text{Re}_{\text{p}} \ll 1$. However, as discussed in Ref. [19], the magnitudes of fluid inertial and Jeffery torques scale differently,

$$\frac{|\boldsymbol{T}_I|}{|\boldsymbol{T}_J|} \sim \frac{|\boldsymbol{u} - \boldsymbol{v}_{\text{p}}|^2}{|\boldsymbol{\omega}/2 - \boldsymbol{\omega}_{\text{p}}|\gamma}, \tag{A13}$$

suggesting that the fluid inertial torque cannot be neglected even in the limit of $\text{Re}_{\text{p}} \ll 1$. Therefore, in the following derivation, we neglect the inertial correction for the drag force but still keep the inertial torque.

Using Eqs. (A1)–(A10), we obtain the governing equations of the particle motion [20],

$$\frac{d\boldsymbol{v}'_{\rm p}}{dt} = \frac{1}{\rm St}\Bigg[\mathbb{A}(\boldsymbol{u}' - \boldsymbol{v}'_{\rm p}) + \frac{F_{\rm swim}\tau_{\rm p}}{m_{\rm p}u_\eta}\boldsymbol{n} + \frac{(\rho_{\rm p}-\rho_{\rm f})g\tau_p}{\rho_{\rm p}u_\eta}\boldsymbol{e}_g\Bigg], \tag{A14}$$

$$\frac{d\boldsymbol{\omega}'_{\rm p}}{dt} = \frac{1}{\rm St}\Bigg[\mathbb{I}_p^{-1}\mathbb{C}'\left(\frac{1}{2}\boldsymbol{\omega}' - \boldsymbol{\omega}'_{\rm p}\right) + \mathbb{I}_p^{-1}\mathbb{H}' : \mathbb{S}' + \mathcal{A}[\boldsymbol{n}\cdot(\boldsymbol{v}'_{\rm p}-\boldsymbol{u}')][\boldsymbol{n}\wedge(\boldsymbol{v}'_{\rm p}-\boldsymbol{u}')]\Bigg] + \frac{\lambda^2-1}{\lambda^2+1}(\boldsymbol{n}\cdot\boldsymbol{\omega}'_{\rm p})(\boldsymbol{\omega}'_{\rm p}\wedge\boldsymbol{n}). \tag{A15}$$

Here, quantities with primes are nondimensionalized by Kolmogorov velocity scale u_η and timescale τ_η. We note that the inertial force correction $\boldsymbol{F}_I$ has been neglected for the derivation of Eq. (A14) with $\mathrm{Re}_{\rm p} \ll 1$, and we use the relationship $d(\mathbb{I}_p\boldsymbol{\omega}_p)/dt = \mathbb{I}_p d\boldsymbol{\omega}_p/dt + \boldsymbol{\omega}_p \wedge (\mathbb{I}_p\boldsymbol{\omega}_p)$ in Eq. (A15). The Stokes number $\mathrm{St} = \tau_{\rm p}/\tau_\eta$ quantifies the inertia of the swimmer, where $\tau_{\rm p} \equiv (2a^2\lambda\rho_{\rm p})/(9\gamma\rho_{\rm f})$ is the particle translational response time, and τ_η is the Kolmogorov timescale. For typical plankton species, St is usually much smaller than unity, as shown in Table II. In the limit of $\mathrm{St} \ll 1$, i.e., the overdamped limit [20], Eqs. (A14) and (A15) can be further simplified,

$$\boldsymbol{v}_{\rm p} = \boldsymbol{u} + v_{\rm swim}\boldsymbol{n} + \boldsymbol{v}_{\rm settle}, \tag{A16a}$$

$$\boldsymbol{\omega}_{\rm p} = \frac{1}{2}\boldsymbol{\omega} + \Lambda(\boldsymbol{n}\wedge\mathbb{S}\cdot\boldsymbol{n}) + \frac{M}{\gamma}[\boldsymbol{n}\cdot(\boldsymbol{v}_{\rm p}-\boldsymbol{u})][\boldsymbol{n}\wedge(\boldsymbol{v}_{\rm p}-\boldsymbol{u})], \tag{A16b}$$

$$\text{where } v_{\rm swim}\boldsymbol{n} = \frac{F_{\rm swim}\tau_{\rm p}}{m_{\rm p}}A_\parallel^{-1}\boldsymbol{n}, \tag{A16c}$$

$$\text{and } \boldsymbol{v}_{\rm settle} = \frac{\rho_{\rm p}-\rho_{\rm f}}{\rho_{\rm p}}g\tau_{\rm p}\mathbb{A}^{-1}\boldsymbol{e}_g. \tag{A16d}$$

In the present study, we directly assign the value of $v_{\rm swim}$, and we use an equivalent definition of $\boldsymbol{v}_{\rm settle}$ [24],

$$\boldsymbol{v}_{\rm settle} = -v_1\boldsymbol{e}_y - (v_3 - v_1)(\boldsymbol{e}_y\cdot\boldsymbol{n})\boldsymbol{n}, \tag{A16e}$$

$$\text{with } \boldsymbol{e}_y = -\boldsymbol{e}_g,$$

$$v_1 = \frac{\rho_{\rm p}-\rho_{\rm f}}{\rho_{\rm p}}g\tau_{\rm p}A_\perp^{-1},$$

$$v_3 = \frac{\rho_{\rm p}-\rho_{\rm f}}{\rho_{\rm p}}g\tau_{\rm p}A_\parallel^{-1},$$

where v_1 and v_3 are the terminal settling speeds of a spheroid in quiescent fluid, with symmetry axis perpendicular and parallel to gravity direction, respectively.

Using Eqs. (A16), we obtain the governing equation of the angular velocity of a settling swimmer [Eq. (4)]. The shape parameter M in Eq. (A16b) is only a function of aspect ratio λ (Fig. 5), and is defined by $M = \mathcal{A}I_\perp/C_\perp$, where $I_\perp$ and $C_\perp$

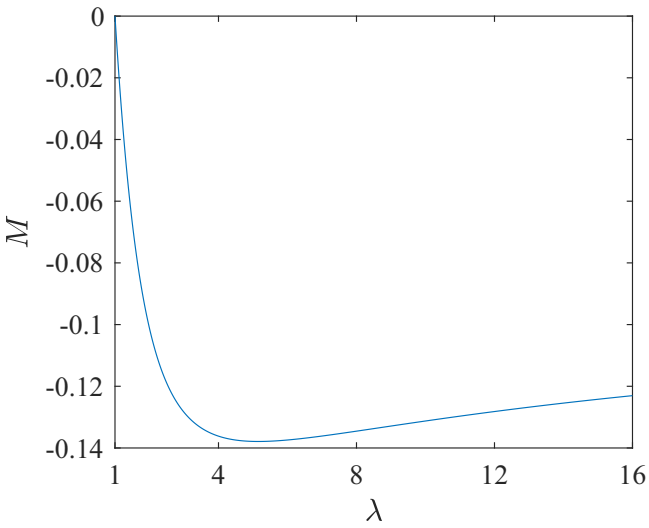

FIG. 5. Shape factor M as a function of aspect ratio λ.

for elongated spheroids are as follows [20]:

$$I_\perp = \frac{1+\lambda^2}{5}a^2, \tag{A17a}$$

$$C_\perp = \frac{8a^2(\lambda^4-1)}{9\lambda[(2\lambda^2-1)\beta-1]}, \tag{A17b}$$

$$\text{with } \beta = \frac{\ln(\lambda+\sqrt{\lambda^2-1})}{\lambda\sqrt{\lambda^2-1}}. \tag{A17c}$$

For elongated spheroids,

$$\mathcal{A} = \frac{5}{6\pi}F_\beta\frac{\lambda^3}{\lambda^2+1}, \tag{A17d}$$

with F_β defined as [21]

$$F_\beta = -\frac{\pi e^2(420e+2240e^3+4249e^5-2152e^7)}{315[(e^2+1)\tanh^{-1}e-e]^2[(1-3e^2)\tanh^{-1}e-e]} + \frac{\pi e^2(420+3360e^2+1890e^4-1470e^6)\tanh^{-1}e}{315[(e^2+1)\tanh^{-1}e-e]^2[(1-3e^2)\tanh^{-1}e-e]} - \frac{\pi e^2(1260e-1995e^3+2790e^5-1995e^7)(\tanh^{-1}e)^2}{315[(e^2+1)\tanh^{-1}e-e]^2[(1-3e^2)\tanh^{-1}e-e]}, \tag{A18}$$

where $e = \sqrt{1-\lambda^{-2}}$. For more details on these parameters, readers can refer to Refs. [19–21].

APPENDIX B: DIRECT NUMERICAL SIMULATION OF TURBULENCE AND SWIMMERS

We use an Eulerian-Lagrangian method to simulate swimmers in homogeneous isotropic turbulence. The dynamics of the fluid phase is resolved in an Eulerian frame, while each individual swimmer is tracked along the Lagrangian trajectory using local instantaneous flow information at the swimmer

position. The incompressible turbulence is directly simulated by solving the Navier-Stokes equations,

$$\frac{\partial \boldsymbol{u}}{\partial t} + \boldsymbol{u}\cdot\nabla\boldsymbol{u} = -\frac{\nabla p_{\mathrm{f}}}{\rho} + \gamma\nabla^2\boldsymbol{u} + \boldsymbol{F}, \tag{B1}$$

$$\nabla\cdot\boldsymbol{u} = 0, \tag{B2}$$

where t is the time and $\boldsymbol{u}$ is the fluid velocity. The symbols p_{f} and ρ denote the pressure and density of fluid, respectively. An external force $\boldsymbol{F}$ is applied to the large scales and injects energy in order to sustain turbulence and balances the rate of viscous dissipation at the Kolmogorov scale η [36]. Three-dimensional periodic boundary conditions are applied on the boundaries of the cubic domain with a size $(2\pi)^3$. A pseudospectral method is used for solving the Navier-Stokes equations, and the 3/2 rule is utilized to reduce the aliasing error on the nonlinear term. The turbulence Taylor-Reynolds number is $\mathrm{Re}_\lambda = u_{\mathrm{rms}}L_\lambda/\gamma = 60$, where u_{rms} is the root-mean-square velocity, $L_\lambda = u_{\mathrm{rms}}\sqrt{15\gamma\epsilon^{-1}}$. We use 96^3 grid points to resolve the turbulent flow fluctuation. The maximum wave number resolved is about 1.78 times greater than the Kolmogorov wave number to ensure the accuracy of resolution at small scales [37]. A random flow with an exponent energy spectrum is given as the initial flow field, and we use an explicit second-order Adams-Bashforth scheme for the time integration of Eqs. (B1) and (B2) with a time step smaller than $0.01\tau_\eta$ [38].

After turbulence is fully developed, swimmers are released in the flow field with random positions and orientations. Fluid velocity and its gradients in Eqs. (2) and (4) are interpolated by a second-order Lagrangian method at the particle position, using fluid information at Eulerian grid points. Equations (1) and (2) are integrated by a second-order Adams-Bashforth scheme similar to time integration of the fluid phase. The number of particles is 120 000 for each parameter configuration, and the statistics in turbulence are obtained by averaging over more than 40 uncorrelated time samples after the statistics has reached a steady state.

APPENDIX C: TYPICAL PARAMETERS OF PLANKTON

Here, we summarize the parameters of typical plankton species [27,28,39–41]. In Table I, we show the typical length, aspect ratio, and swimming and settling speeds. In Table II, we summarize the nondimensional parameters. The Re_{p} and St of these typical species are negligibly small, so the model derived in Appendix A is applicable. We also estimate the reorientation parameter Ψ_I with Eq. (11). Ψ_I is small for fast-swimming species in turbulence with small energy dissipation rate, indicating that the effect of fluid inertial torque is significant.

[1] T. J. Smayda, Harmful algal blooms: Their ecophysiology and general relevance to phytoplankton blooms in the sea, Limnol. Oceanogr. **42**, 1137 (1997).

[2] G. C. Hays, A review of the adaptive significance and ecosystem consequences of zooplankton diel vertical migrations, *Migrations and Dispersal of Marine Organisms* (Springer, Dordrecht, 2003), p. 163.

[3] S. M. Bollens and B. Frost, Predator-induced diet vertical migration in a planktonic copepod, J. Plankton Res. **11**, 1047 (1989).

[4] O. Pundyak, Possible means of overcoming sedimentation by motile sea-picoplankton cells, Oceanologia **59**, 108 (2017).

[5] B. Eggersdorfer and D.-P. Häder, Phototaxis, gravitaxis and vertical migrations in the marine dinoflagellate prorocentrum micans, FEMS Microbiol. Lett. **85**, 319 (1991).

[6] R. Stocker, J. R. Seymour, A. Samadani, D. E. Hunt, and M. F. Polz, Rapid chemotactic response enables marine bacteria to exploit ephemeral microscale nutrient patches, Proc. Natl. Acad. Sci. USA **105**, 4209 (2008).

[7] J. O. Kessler, Individual and collective fluid dynamics of swimming cells, J. Fluid Mech. **173**, 191 (1986).

[8] A. M. Roberts, Geotaxis in motile micro-organisms, J. Expt. Biol. **53**, 687 (1970).

[9] S. Lovecchio, E. Climent, R. Stocker, and W. M. Durham, Chain formation can enhance the vertical migration of phytoplankton through turbulence, Sci. Adv. **5**, eaaw7879 (2019).

[10] W. M. Durham, J. O. Kessler, and R. Stocker, Disruption of vertical motility by shear triggers formation of thin phytoplankton layers, Science **323**, 1067 (2009).

[11] A. Sengupta, F. Carrara, and R. Stocker, Phytoplankton can actively diversify their migration strategy in response to turbulent cues, Nature (London) **543**, 555 (2017).

[12] W. M. Durham, E. Climent, M. Barry, F. De Lillo, G. Boffetta, M. Cencini, and R. Stocker, Turbulence drives microscale patches of motile phytoplankton, Nat. Commun. **4**, 2148 (2013).

[13] F. De Lillo, M. Cencini, W. M. Durham, M. Barry, R. Stocker, E. Climent, and G. Boffetta, Turbulent Fluid Acceleration Generates Clusters of Gyrotactic Microorganisms, Phys. Rev. Lett. **112**, 044502 (2014).

[14] C. Zhan, G. Sardina, E. Lushi, and L. Brandt, Accumulation of motile elongated micro-organisms in turbulence, J. Fluid Mech. **739**, 22 (2014).

[15] K. Gustavsson, F. Berglund, P. R. Jonsson, and B. Mehlig, Preferential Sampling and Small-Scale Clustering of Gyrotactic Microswimmers in Turbulence, Phys. Rev. Lett. **116**, 108104 (2016).

[16] M. Borgnino, G. Boffetta, F. De Lillo, and M. Cencini, Gyrotactic swimmers in turbulence: Shape effects and role of the large-scale flow, J. Fluid Mech. **856**, R1 (2018).

[17] I. Fouxon and A. Leshansky, Phytoplankton's motion in turbulent ocean, Phys. Rev. E **92**, 013017 (2015).

[18] D. Lewis, The orientation of gyrotactic spheroidal microorganisms in a homogeneous isotropic turbulent flow, Proc. R. Soc. London, Ser. A **459**, 1293 (2003).

[19] M. Z. Sheikh, K. Gustavsson, D. Lopez, E. Lévêque, B. Mehlig, A. Pumir, and A. Naso, Importance of fluid inertia for the orientation of spheroids settling in turbulent flow, J. Fluid Mech. **886**, A9 (2020).

[20] K. Gustavsson, M. Z. Sheikh, D. Lopez, A. Naso, A. Pumir, and B. Mehlig, Effect of fluid inertia on the orientation of a small prolate spheroid settling in turbulence, New J. Phys. **21**, 083008 (2019).

[21] V. Dabade, N. K. Marath, and G. Subramanian, Effects of inertia and viscoelasticity on sedimenting anisotropic particles, J. Fluid Mech. **778**, 133 (2015).

[22] H. Brenner, The Oseen resistance of a particle of arbitrary shape, J. Fluid Mech. **11**, 604 (1961).

[23] G. B. Jeffery, The motion of ellipsoidal particles immersed in a viscous fluid, Proc. R. Soc. London, Ser. A **102**, 161 (1922).

[24] S. Kim and S. J. Karrila, *Microhydrodynamics: Principles and Selected Applications* (Butterworth-Heinemann, Boston, 1991).

[25] S. O'Malley and M. Bees, The orientation of swimming biflagellates in shear flows, Bull. Math. Biol. **74**, 232 (2012).

[26] T. J. Pedley and J. Kessler, The orientation of spheroidal microorganisms swimming in a flow field, Proc. R. Soc. London B **231**, 47 (1987).

[27] T. J. Smayda, Adaptations and selection of harmful and other dinoflagellate species in upwelling systems. 2. Motility and migratory behaviour, Prog. Oceanogr. **85**, 71 (2010).

[28] J. Titelman and T. Kiørboe, Motility of copepod nauplii and implications for food encounter, Marine Ecol. Prog. Ser. **247**, 123 (2003).

[29] D. Kamykowski, R. E. Reed, and G. J. Kirkpatrick, Comparison of sinking velocity, swimming velocity, rotation and path characteristics among six marine dinoflagellate species, Marine Biol. **113**, 319 (1992).

[30] M. C. Davey and A. E. Walsby, The form resistance of sinking algal chains, Brit. Phycolog. J. **20**, 243 (1985).

[31] F. Candelier, J. Einarsson, and B. Mehlig, Angular Dynamics of a Small Particle in Turbulence, Phys. Rev. Lett. **117**, 204501 (2016).

[32] F. Candelier, B. Mehlig, and J. Magnaudet, Time-dependent lift and drag on a rigid body in a viscous steady linear flow, J. Fluid Mech. **864**, 554 (2019).

[33] H. Brenner, The Stokes resistance of an arbitrary particle, Chem. Eng. Sci. **18**, 1 (1963).

[34] R. Khayat and R. Cox, Inertia effects on the motion of long slender bodies, J. Fluid Mech. **209**, 435 (1989).

[35] S. Kim and S. J. Karrila, *Microhydrodynamics: Principles and Selected Applications* (Courier Corporation, North Chelmsford, Massachusetts, 2013).

[36] L. Machiels, Predictability of Small-Scale Motion in Isotropic Fluid Turbulence, Phys. Rev. Lett. **79**, 3411 (1997).

[37] S. B. Pope, *Turbulent Flows* (IOP Publishing, Bristol, UK, 2001).

[38] R. Rogallo, Numerical Experiments in Homogeneous Turbulence, NASA, NASA Ames Research Center Moffett Field, CA, Report No. 81315, 1981.

[39] M. H. Sohn, K. W. Seo, Y. S. Choi, S. J. Lee, Y. S. Kang, and Y. S. Kang, Determination of the swimming trajectory and speed of chain-forming dinoflagellate cochlodinium polykrikoides with digital holographic particle tracking velocimetry, Marine Biol. **158**, 561 (2011).

[40] J. Titelman, Swimming and escape behavior of copepod nauplii: implications for predator-prey interactions among copepods, Marine Ecol. Prog. Ser. **213**, 203 (2001).

[41] F. Carlotti, D. Bonnet, and C. Halsband-Lenk, Development and growth rates of centropages typicus, Prog. Oceanogr. **72**, 164 (2007).

[42] T. Kiørboe and S. Enric, Planktivorous feeding in calm and turbulent environments, with emphasis on copepods, Marine Ecol. Prog. Ser. **122**, 135 (1995).